Desalination and Water Treatment
www.deswater.com
doi: 10.5004/dwt.2023.29784

306 (2023) 165–177
September

A method for alkali hydrolysis modification of PAN/PES/TiO_2 composite ultrafiltration membranes

Xin Liu, Lei Kong, Xu Zhao, Kunpeng Wu, Zhiyong Tan*

[a]*Engineering Research Center of the Ministry of Education for Synthetic Resins and Special Fibers, Changchun University of Technology, Changchun 310012, Jilin, China, Tel.: +13074350138; email: tanzhiy@163.com (Z.Y. Tan), Tel.: +16604465116; email: 1179563851@qq.com (X. Liu), Tel.: +15755230031; email: 2160470021@qq.com (L. Kong), Tel.: +18843569565; email: 1342022011@qq.com (X. Zhao), Tel.: +18848005475; email: 1274368751@qq.com (K.P. Wu)*
[b]*College of Chemical Engineering, Changchun University of Technology, Changchun 310012, Jilin, China*

Received 10 May 2023; Accepted 17 July 2023

ABSTRACT

In this work, we prepared polyacrylonitrile/polyethersulfone/TiO_2 (PAN/PES/TiO_2) composite ultrafiltration membranes using the immersed phase conversion method and used alkali hydrolysis modification to prepare a modified ultrafiltration membrane with high water flux, good hydrophilicity, and excellent anti-pollution properties. The composite ultrafiltration membrane was characterized by an infrared spectrometer, differential scanning calorimeter, scanning electron microscope, contact angle tester, UV spectrophotometer, membrane performance evaluation instrument, and other characterization means to perform a full range of performance tests. The results showed that the water flux of the prepared PAN/PES/TiO_2 composite ultrafiltration membrane was as high as 619.4 L/m^2·h, and the rejection rate of bovine serum albumin was 95.78%, which reached the ideal level. In this study, PAN/PES ultrafiltration membrane, PAN/PES hydrolysis membrane, PAN/PES/TiO_2 ultrafiltration membrane, and PAN/PES/TiO_2 hydrolysis ultrafiltration membrane were also tested for anti-pollution stability and filtration flux stability in comparison. The final test results showed that the PAN/PES/TiO_2 hydrolysis ultrafiltration membrane had excellent anti-pollution stability and performed the best in long-term flux. The final results showed that PAN/PES/TiO_2 hydrolyzed ultrafiltration membranes had excellent anti-pollution stability and performed best in long-term flux stability tests.

Keywords: Ultrafiltration membrane; Anti-pollution; Alkali hydrolysis; TiO_2 nanoparticles; Polyacrylonitrile

1. Introduction

Water contamination is currently putting the entire world to the test. Without question, developing countries bear the burden of this dilemma [1,2]. Economic development and human activities will eventually harm the global environment and climate. The world will avoid extreme freshwater scarcity with appropriate responses shortly [3–5]. For these reasons, many researchers are investigating methods to filter wastewater, and membrane separation technology has evolved. This technology has quickly grown as an easy-to-use, extensively employed, and environmentally friendly technology that has permeated various businesses worldwide [6–8]. While providing economic benefits, membrane separation technology has also considerably reduced the problem of water scarcity caused by water contamination. Because the commonly used ultrafiltration membrane substrates polyethersulfone (PES) and polysulfone (PSF) have poor hydrophilicity and serious membrane contamination issues [9–14], an increasing number of researchers are

* Corresponding author.

using polyacrylonitrile (PAN) with hydrophilic groups as membrane substrates to prepare ultrafiltration membranes. PAN is a low-cost polymer with strong solvent and chlorine resistance. PAN also offers specific advantages. PAN is a low-cost polymer with excellent solvent and chlorine resistance and hydrophilic and flexible qualities. It is ideal for use as a membrane-forming substrate in water purification technology [15–17]. PAN has poor chemical stability and mechanical properties during film formation [13]. There is already research in the literature to address these issues, and one of the easiest and most effective solutions is to combine PAN with another polymer with complementary advantages to compensate for the shortcomings of PAN [18–21]. This can highlight the benefits of both materials and eliminate any defects in single-component materials. These requirements are precisely met by polyethersulfone (PES), a high-performance thermoplastic with exceptional thermal and mechanical stability [22,23]. This co-blending method to create composite substrate membranes is preferable to ultrafiltration membranes using a single material as the membrane substrate.

Although PAN and PES have excellent physicochemical properties, their hydrophilicity does not reach the expected level when used as membrane substrates in ultrafiltration membranes. Low ultrafiltration membrane water flux and serious membrane contamination issues can result from low hydrophilicity. Membrane contamination has long been a problem in membrane water treatment technology. This is because ultrafiltration membrane contamination resistance determines their application scope and service life, and ultrafiltration membranes with high contamination resistance can significantly reduce operating costs, maintenance time, and energy consumption [24–26]. To improve the contamination resistance of ultrafiltration membranes, one frequent strategy is to increase the hydrophilicity of the membrane through a series of modifications, among which the decreased hydrolysis method is one of the most common. Wang et al. [27] prepared PAN/$ZnCl_2$ composite nanofiltration membranes and discovered that after soaking for a certain period in 1 M NaOH robust alkali solution, the pore size on the membrane surface was reduced and more uniformly distributed. These changes significantly improve the pollution resistance of the ultrafiltration membrane while maintaining the composite membrane water flux without adverse effects. Zhang et al. [28] hydrolytically modified the PAN ultrafiltration membrane using 2 M NaOH, KOH, and the Atomic Force Microscope (AFM) test results showed that the hydrolysis reaction resulted in the formation of a smoother surface of the PAN ultrafiltration membrane, which is essential for improving the contamination resistance of ultrafiltration membranes. However, using a high concentration of alkali solution to treat the ultrafiltration membrane is likely to cause damage to the membrane structure, necessitating careful control of the reaction temperature and time, and using such a high concentration of solid alkali solution to modify the ultrafiltration membrane carries certain safety risks and is not suitable for mass production in plants.

Although many studies have reported that reacting PAN with alkali solutions such as NaOH, KOH, and LiOH using alkali hydrolysis to generate more hydrophilic amide and carboxylic acid groups can indeed improve the hydrophilicity of ultrafiltration membranes [29,30], this method inevitably damages the mechanical properties of the ultrafiltration membrane [31], exacerbating the poor mechanical properties of the PAN ultrafiltration membrane. To address this issue, some researchers have found that adding hydrophilic nanoparticles to the membrane matrix can effectively improve the fouling resistance and mechanical properties of ultrafiltration membranes [32–35]. Zhang et al. [36] successfully encapsulated TiO_2 nanoparticles on the surface of PSF ultrafiltration membranes using a surface coating approach. The final results showed that the modified ultrafiltration membrane performed significantly better regarding contaminant resistance and mechanical qualities than the pristine PSF ultrafiltration membrane. However, the water flux was lowered by 40.66%. This modification method improved the contamination resistance of ultrafiltration membranes at the expense of reducing the water flux. Still, the modification method using surface coating needs to be simplified, and the modification conditions are demanding, limiting the applicability of the modified membranes. Rahimpour et al. [37] prepared PES/TiO_2 encapsulated membranes, UV-irradiated PES/TiO_2 encapsulated membranes, and UV-irradiated PES/TiO_2 co-blended membranes, and the test results revealed that the added modified membranes improved contamination resistance and long-term flux stability compared to pure PES ultrafiltration membranes.

We created PAN/PES/TiO_2 hybrid ultrafiltration membranes by adding a specific quantity of TiO_2 nanoparticles to the PAN/PES ultrafiltration membrane matrix using a straightforward co-blending modification technique. Including TiO_2 nanoparticles, many hydroxyl groups ($^-$OH) were added to improve the hydrophilicity and self-cleaning ability of the composite membrane. Simultaneously, the modification conditions were adjusted, and the PAN/PES/TiO_2 hybrid ultrafiltration membrane was changed by alkali hydrolysis using a low concentration of NaOH solution to explore the optimum modification conditions. This study prepared a series of PAN/PES/TiO_2 composite ultrafiltration membranes with various modification conditions, and in-depth research was conducted on the effect of hydrolysis temperature on the performance of different ultrafiltration membranes. The final ultrafiltration membranes were distinguished by significant water flux, good hydrophilicity, powerful anti-pollution performance, and high long-term flux stability. The preparation method of PAN/PES/TiO_2 composite ultrafiltration membrane and the modification principle is shown in Fig. 1.

2. Materials and methods

2.1. Materials

Polyacrylonitrile (PAN, PDI = 1.97, Mw = 15,000) polymer dispersity index (PDI) and polyethylene glycol 1000 (PEG, PDI = 1.03, Mw = 1,000), purchased from Shanghai Maclean Biochemical Technology Co., (Shanghai, China). Polyethersulfone (PES, PDI = 2.53, Mw = 58,000), purchased from Solvay Limited (Shanghai, China). N,N-dimethylacetamide (DMAc), purchased from Tianjin Fuyu Fine Chemical Co., Ltd., (Tianjin, China). Sodium hydroxide (NaOH), purchased from Tianjin Chemical Reagent Co., Ltd., (Tianjin, China).

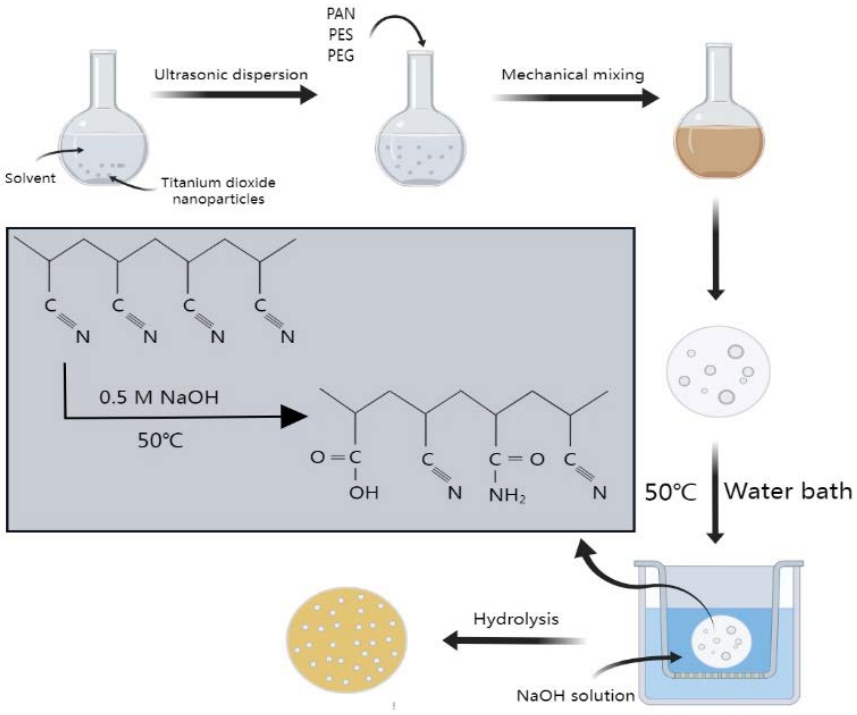

Fig. 1. Preparation method of PAN/PES/TiO_2 composite ultrafiltration membrane and schematic diagram of the modification principle.

Bovine serum albumin (BSA, 66 kDa), purchased from Beijing Dingguo Biological Co., Ltd., (Beijing, China). Titanium dioxide nanoparticles (TiO_2, 99.8% metals basis, 20 nm primary particle size, Mw = 79.87), purchased from Shanghai Maclean Biochemical Technology Co., (Shanghai, China).

2.2. Preparation of PAN/PES/TiO_2 composite ultrafiltration membrane

First, PES and PAN were vacuum dried for 8 h to ensure complete elimination of water. A certain amount of TiO_2 (2 wt.%) nanoparticles were mixed with DMAc. After 1 h of ultrasonic shock, the ultrasonic dispersion was transferred to a three-post round-bottom flask, and PAN (14 wt.%), PES (3 wt.%), and PEG (5 wt.%) were added quantitatively in turn. The three-post round-bottom flask was placed in a constant temperature water bath at 80°C for 12 h with mechanical stirring to obtain a transparent and uniform cast film solution. The cast film solution is then defoamed at room temperature for 12 h before being poured uniformly onto a dry, clean, smooth glass plate with a wet film applicator and scraped into a liquid film of uniform thickness (film thickness of 150 μm). After the 30 s of waiting for the solvent in the liquid membrane to evaporate, the liquid membrane is instantly transferred to a solidification bath made of distilled water to enable the solvent exchange to occur, resulting in the final ultrafiltration membrane. After the membrane has been completely peeled off the glass plate, the composite ultrafiltration membrane is immersed in deionized water for 72 h to guarantee total solvent removal from the membrane before being immersed in fresh distilled water for testing.

2.3. Preparation of PAN/PES/TiO_2 film modified by sodium hydroxide

Soak the PAN/PES/TiO_2 composite membrane in NaOH solution for 45 min at 40°C, 45°C, 50°C, 55°C, and 60°C. After soaking, the membrane surface was thoroughly washed with distilled water. After soaking, the membrane surface was rinsed with distilled water until neutral and carefully kept in distilled water for measurement. Following that, the unhydrolyzed PAN/PES/TiO_2 ultrafiltration membrane as M0, the ultrafiltration membrane hydrolyzed for 40°C as M1, the ultrafiltration membrane hydrolyzed for 45°C as M2, the ultrafiltration membrane hydrolyzed for 50°C as M3, the ultrafiltration membrane hydrolyzed for 55°C as M4, the ultrafiltration membrane hydrolyzed for 60°C as M5. For the convenience of subsequent description, the PAN/PES ultrafiltration membrane without TiO_2 nanoparticles is recorded as M6, the PAN/PES ultrafiltration membrane after 45 min treatment with alkali solution at 50°C is recorded as M7, the PAN/TiO_2 ultrafiltration membrane as M8 and the PES/TiO_2 ultrafiltration membrane as M9.

2.4. Test method

2.4.1. Pure water flux test

A membrane performance evaluation equipment was used to measure the pure water flux of a composite ultrafiltration membrane. The membrane was put into the device at room temperature, the pressure was adjusted to 0.1 MPa, and the pressure was pre-compression for 15 min. The permeable liquid volume was measured every 3 min once the

pressure and flow rate were stabilized. The pure water permeability (J_w) of the membranes was calculated by Eq. (1):

$$J_w = \frac{V}{S_1 \times \Delta t} \tag{1}$$

where J_w is the pure water permeability (L/m²·h); V is the volume of water passing through the ultrafiltration membrane (L); S_1 is the effective filtration area (m³); Δt is the collection time (h).

2.4.2. Retention test

A membrane performance evaluation equipment was used to test the retention rate of a composite ultrafiltration membrane. As the polluted liquid, a 0.1 g/L BSA solution was created. After inserting the membrane into the instrument, the pressure was reduced to 0.1 MPa. After stabilizing the pressure and flow rate at room temperature for 10 min, the polluted liquid was continued for 10 min, and the filtrate was collected. The retention rate (R) of the membranes was calculated by Eq. (2).

$$R = \left(1 - \frac{C_1}{C_0}\right) \times 100\% \tag{2}$$

where C_0 is the absorbance of BSA in feeding liquid; C_1 is the absorbance of BSA infiltrate. In this experiment, C_0 and C_1 were obtained from the ultraviolet absorbance at 278.5 nm.

2.4.3. Structural characterization

Before the test, the film should be sliced into splines of a specific size, and the splines should be washed with deionized water before being frozen and broken in liquid nitrogen. Using gold spraying equipment, a small layer of gold was sprayed on the surface of the ultrafiltration membrane, and the membrane structure was then examined using a scanning electron microscope.

Ultrafiltration membrane chemical composition characterization: The chemical composition of the ultrafiltration membrane was investigated using an infrared spectrometer before and after modification, as well as the impact of varied hydrolysis times on the chemical composition of the ultrafiltration membrane. The film should be dry before the test. The Attenuated Total Refraction (ATR) measuring mode was employed, with a measurement range 4,000–400 cm^{-1} and a resolution of 4 cm^{-1}.

2.4.4. Porosity test

The gravimetric method was used to determine the porosity of the ultrafiltration membrane. The film was sliced into 3 cm × 3 cm pieces, and the surplus water on the surface was gently wiped away using dust-free absorbent paper. The thickness of the film was measured and weighed using an electronic display caliper, designated as W_1. The film was soaked in anhydrous ethanol for 8 h before being dried in a vacuum drying oven for 24 h. After the film had completely dried, it was weighed and labeled W_2. The porosity (Pr) of the membranes was calculated by Eq. (3).

$$\mathrm{Pr} = \frac{w_1 - w_2}{V_m \times \rho} \tag{3}$$

where W_1 is the composite film wet weight (g); W_2 is the composite film dry weight (g); V_m is the composite membrane volume (cm³); ϱ is the water density (g/cm³).

2.4.5. Water absorption rate test

Cut the film into small 2 cm × 2 cm pieces. After soaking in deionized water for a day at room temperature, wipe off excess water with dust-free absorbent paper and weigh it, designated as W_w. The diaphragm was placed in a vacuum drying oven and dried at 60°C for 12 h before being considered and denoted as W_d. The water absorption rate (W) of the membranes was calculated by Eq. (4).

$$W = \frac{w_w - w_d}{W_d} \times 100\% \tag{4}$$

where W_w is the ultrafiltration membrane wet weight (g); W_d is the ultrafiltration membrane dry weight (g).

2.4.6. Test of static adsorption capacity

The ultrafiltration membrane was sliced into 3 cm × 3 cm sample pieces and treated in a 0.1 g/L bovine serum albumin solution. After being enclosed and soaked for 12 h at room temperature, the absorbance of the leftover liquid at 278.5 nm was measured using an ultraviolet spectrophotometer. Convert absorbance to concentration using commonly used working curve formulas and estimate the static adsorption capacity Q of the ultrafiltration membrane. The standard working curve calculation Eq. (5) and the static adsorption capacity (Q) calculation Eq. (6) are as follows.

$$C = (A \times 682.682) + 18.98304 \tag{5}$$

where C is the solution concentration (mg/L); A is the absorbance of the solution at 278.5 nm.

$$Q = \frac{V_1\left(C_0 - C_1\right)}{S_2} \tag{6}$$

where Q is the static adsorption capacity (mg/cm²); V_1 is the volume of BSA solution (L); C_0 is the initial concentration of BSA solution (mg/L); C_1 is the BSA residual solution concentration (mg/L); S_2 is the ultrafiltration membrane area (cm²).

2.4.7. Dynamic pollution test

The dynamic pollution test method was utilized to evaluate the anti-pollution property of alkali hydrolyzed modified ultrafiltration membrane using BSA solution (1 g/L) as the pollution solution. After inserting the membrane into the instrument, the pressure was reduced to 0.1 MPa, and deionized water was filtered for 0.5 h. The water flux, designated as J_0, was measured every 3 min during this

operation. The deionized water was then replaced with BSA solution, and the filtering experiment was carried out for 0.5 h at 0.1 MPa. The flux, designated as J_s, was measured every 3 min during this operation.

Using the BSA solution (1 g/L) as a pollution solution, a dynamic pollution test method was used to investigate the anti-pollution property of the alkali hydrolyzed modified ultrafiltration membrane. After the membrane was embedded in the instrument, the pressure was adjusted to 0.1 MPa, and the filtration was carried out with deionized water for 0.5 h. During this process, the water flux was recorded every 3 min, denoted as J_0. Then, the deionized water was changed into BSA solution, and the filtration experiment was carried out at 0.1 MPa for 0.5 h. In this process, the flux was recorded every 3 min, denoted as J_s. The ultrafiltration membrane was removed, and deionized water was used to wash the contaminants adhering to the membrane surface for 10 min. Then, deionized water was used for a 0.5 h filtration experiment. The flux was monitored every 3 min during this operation and labeled J_1.

The following three ratios were defined in this study to characterize the anti-pollution performance of ultrafiltration membrane in detail to more intuitively depict the anti-pollution capabilities of ultrafiltration membrane:

$$m = \frac{J_0 - J_1}{J_1} \tag{7}$$

where m is the total pollution coefficient of the ultrafiltration membrane, it describes the decrease of membrane flux after the pollution of the ultrafiltration membrane.

$$\mathrm{Rr} = \frac{J_1 - J_s}{J_0} \tag{8}$$

where Rr is the reversible pollution coefficient of ultrafiltration membrane (%), which can be removed by cleaning.

$$\mathrm{Rir} = \frac{J_0 - J_1}{J_0} \tag{9}$$

where Rir is the irreversible pollution coefficient of ultrafiltration membrane (%), which is permanent and cannot be removed by artificial means.

2.4.8. Hydrophilicity test

The surface hydrophilicity of ultrafiltration membranes is measured using a contact angle tester. To ensure that the water contained in the ultrafiltration membrane is entirely removed, the membrane should be sliced into strips of a specific size and dried in an oven for 24 h before the test. The strips are then placed on a clean slide, and the contact angle is measured by using a tiny syringe to administer a drop of deionized water to the membrane surface. At least five different places were chosen and averaged for each sample strip.

2.4.9. Thermal analysis

Perform thermal analysis of the ultrafiltration membrane using differential scanning calorimeter (DSC). Before testing, place the wet film in a vacuum oven at 60°C and thoroughly dry for 24 h. Heat approximately 8mg of the sample in nitrogen at 10°C/min from 25°C to 400°C. When detecting the glass transition temperature (T_g), take a piece of about 8 mg and heat it in nitrogen at 40°C/min from 0°C to 280°C.

2.4.10. Anti-pollution stability test

The anti-pollution stability of the ultrafiltration membrane was investigated using three cycles of dynamic contamination testing. After embedding the membrane in the apparatus, the pressure was reduced to 0.1 MPa, and deionized water was utilized for 0.5 h of filtration, with the water flux measured every 3 min. The deionized water was subsequently replaced with a solution of BSA (1 g/L), and the filtration experiment was carried out for 0.5 h at 0.1 MPa pressure, with the flux recorded every 3 min. The membrane was removed, and the pollutants adhered to the membrane surface were washed with deionized water for 10 min before repeating the filtering experiment with deionized water for 0.5 h for 30 min, with flux recorded every 3 min. The preceding procedure is a single cycle of anti-pollution testing; following the test, the initial processes will be repeated three times to evaluate changes in the filtration flow of each component ultrafiltration membrane. All four types of ultrafiltration membranes during the trial should be measured three times, and the average value should be taken.

2.4.11. Performance stability test

The PAN/PES ultrafiltration membrane, PAN/PES hydrolysis membrane, PAN/PES/TiO_2 ultrafiltration membrane, and PAN/PES/TiO_2 hydrolysis membrane were immersed in deionized water and then placed in the same manner for three months and six months to test the dynamic anti-pollution performance of the membranes and observe whether the anti-pollution performance of the membranes had decreased. During the placement procedure, the deionized water must be replaced once a month, all four ultrafiltration membranes must be measured three times, and the average value must be obtained.

3. Results and discussion

3.1. Infrared spectroscopy of ultrafiltration membranes with different components

Fig. 2 shows the infrared spectra of PAN/PES/TiO_2 films and their hydrolysis temperatures. The distinctive peaks of cyano groups showed between 2,244 and 1,440 cm^{-1} in the infrared spectrum of unhydrolyzed PAN/PES/TiO_2, while the characteristic peaks of alkyl fatty groups appeared at 1,733 cm^{-1}. Significant weakening of these polyacrylonitrile distinct peaks was observed after hydrolysis, indicating that the number of cyano groups decreased to some extent under the action of the hydrolysis reaction, and the absorption peak strengths of 1,733 and 1,440 cm^{-1} gradually decreased with increasing hydrolysis temperature. A new band developed in the infrared spectra of PAN hydrolysis at 1,677 cm^{-1}, which is the characteristic peak of sodium polyacrylate, indicating the production of hydrophilic groups. The carboxylic acid (COO^-) groups generate a distinctive

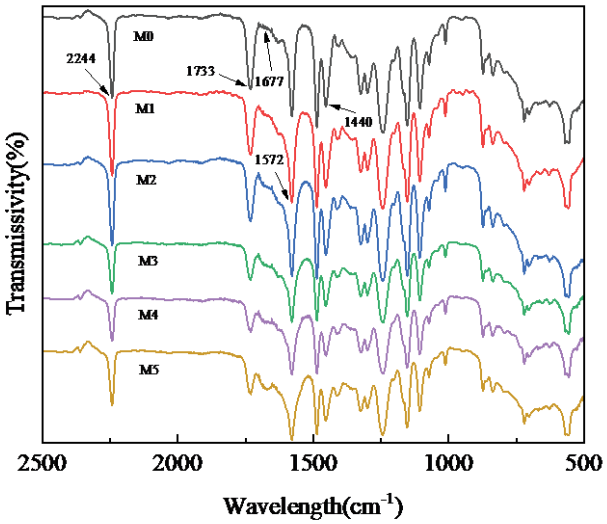

Fig. 2. Infrared spectra for PAN/PES/TiO_2 with different hydrolysis temperatures.

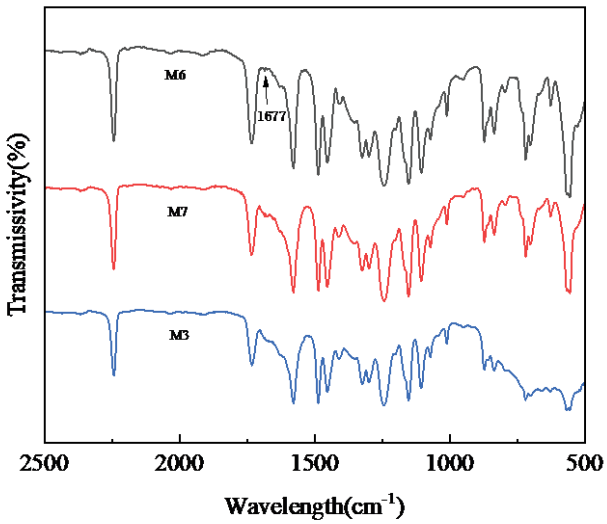

Fig. 3. Infrared spectra for different components of ultrafiltration membrane membranes.

peak at 1,572 cm^{-1}. The strength of the characteristic peaks at 1,572 and 1,677 cm^{-1} gradually increases as the hydrolysis duration increases, showing that the concentration of carboxyl groups gradually increases and the hydrophilicity of the membrane improves. Fig. 3 shows that the hydrolysis degree of M3 is more thorough than that of M7 at the same hydrolysis temperature (50°C) because the infrared absorption peak of M3 is the most obvious at 1,677 cm^{-1}, which is the characteristic peak of sodium polyacrylate. This shows that M3 produces more hydrophilic groups. The insertion of TiO_2 nanoparticles may increase the amount of –OH groups in the associated state in the membrane matrix, hence speeding up the hydrolysis reaction rate. According to prior work results, excessive hydrolysis time can cause irreversible damage to the membrane structure. So obtaining deeper reaction levels in a shorter period will equip the ultrafiltration membrane with better performance.

3.2. Effect of hydrolysis temperature on the degree of PAN cyclization reaction

The DSC curves of PAN/PES/TiO_2 ultrafiltration membranes at different hydrolysis temperatures are shown in Fig. 4, and the specific exothermic values and enthalpies are shown in Table 1. It is not difficult to see that the peak heat release of M0 is the smallest, sharpest, and highest. The peak height lowers after alkaline hydrolysis treatment, and as the hydrolysis temperature rises, the exothermic peak shifts to a lower temperature, resulting in a decrease in the heat of the cyclization process and a gradual spreading of the peak. Introducing amide and carboxyl groups into the ultrafiltration membrane after treatment with an alkaline solution promotes the nucleophilic reaction, increasing the degree of cyclization. The cyanide group in PAN undergoes a cyclization process, which causes the exothermic peak. When the polymer chain degrades, a considerable quantity

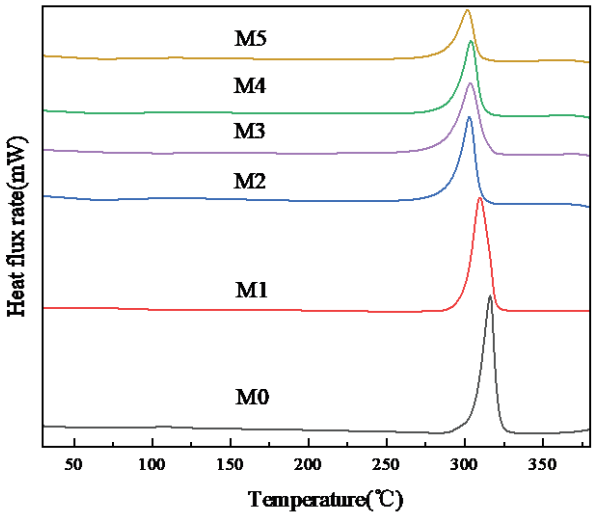

Fig. 4. DSC curves of PAN/PES/TiO_2 ultrafiltration membranes at different hydrolysis temperatures.

Table 1
Characteristic parameters in DSC curves of different ultrafiltration membranes

	Exothermic temperature (°C)	ΔH_c in N_2 (J/g)
M0	309.64	525.48
M1	316.22	513.11
M2	303.51	377.16
M3	302.98	366.76
M4	303.86	319.93
M5	301.75	211.9
M6	307.21	697.63

of heat energy is released, forming a single exothermic peak, as seen in the image. According to the DSC test results, the hydrolyzed ultrafiltration membrane has a lower cyclization temperature and a greater cyclization degree [38–40]. This conclusion is consistent with infrared spectroscopy. Fig. 5 shows the influence of TiO_2 nanoparticles on the DSC curve of the PAN/PES ultrafiltration membrane. As shown in the figure, the amplitude of the exothermic peak of M6 is higher than M0, but the exothermic peak is lower than M0 at 305°C, and the exothermic peak of M6 is slightly wider than M0. It is worth mentioning that filling a small amount of TiO_2 nanoparticles significantly reduces the heat of the cyclization reaction, indicating that adding TiO_2 nanoparticles can prevent the extreme heat release of PAN/PES ultrafiltration membranes, thereby improving thermal stability [41].

3.3. Effect of alkali hydrolysis temperature on ultrafiltration performance of ultrafiltration membrane

The variations in water flow and retention rate of a PAN/PES/TiO_2 composite ultrafiltration membrane under varied hydrolysis temperature settings are depicted in Fig. 6. The experimental results show that as the hydrolysis time rises, the pure water flux of the composite membrane increases first and then quickly falls. In contrast, the interception reduces first and then increases. The maximum water flow at a hydrolysis temperature 50°C is 619.4 L/m^2·h, and the minimum retention rate is 95.78%. Because of the comparatively moderate temperature conditions in the early phases of hydrolysis, soaking the membrane in an alkaline solution below 50°C can perform hydrolysis without damaging the membrane structure, resulting in more hydrophilic carboxylic acid groups. At the same time, TiO_2 nanoparticles, which are hydrophilic inorganic fillers, would naturally aggregate on the surface of the ultrafiltration membrane during the phase transition process, increasing the hydrophilicity of the membrane surface even more [42]. The pure water flux of an ultrafiltration membrane is affected by its surface hydrophilicity, porosity, and overall structure. The composite membrane enters the alkaline solution when the hydrolysis temperature surpasses 50°C, and the membrane structure changes. The diameter of the "small pits" on the membrane surface decreases, and the contact area with water molecules sharply decreases, resulting in a significant decrease in water flux. When the hydrolysis temperature hits 60°C, the ultrafiltration membrane curls due to the overly severe hydrolysis environment, compressing the massive cavity structure in the center of the ultrafiltration membrane. The water flow of the ultrafiltration membrane is currently the lowest, at 180.6 L/m^2·h, while the retention rate is as high as 98.99%.

3.4. Morphological analysis of PAN/PES/TiO_2 films at different hydrolysis temperatures

Fig. 7 shows the effect of hydrolysis time on the surface structure of PAN/PES/TiO_2 ultrafiltration membranes. It can be seen that the diameter of the depressions on the surface of the unhydrolyzed modified ultrafiltration membrane is more significant, and the excavations are deeper. When the hydrolysis temperature is 40°C, the depression niche of the ultrafiltration membrane shrinks, and the diameter of the cavity shrinks from 10 μm to the range of 1~5 μm. In contrast, the depth of depression becomes shallow, and some tiny pores even disappear due to shrinkage. When the hydrolysis temperature was increased to 50°C, the membrane formed an ideal surface structure, and the shrinkage of the diameter of the depressions did not affect the number of nubs. Such a dense nub structure would enhance the surface roughness of the ultrafiltration membrane and increase the contact area between the membrane surface and water molecules, which positively impacted the water flux of the membrane. At the same time, the small diameter and shallow depth of the niche structure are not conducive to the adhesion of contaminants, and the contamination resistance of the ultrafiltration membrane will be improved [31].

The cross-sectional diagrams of PAN/PES/TiO_2 membranes at various hydrolysis temperatures are shown in Fig. 8. As shown in the figure, alkali hydrolysis has a more visible effect on the internal pore structure of the membrane. The finger pores of the original PAN/PES/TiO_2 membrane

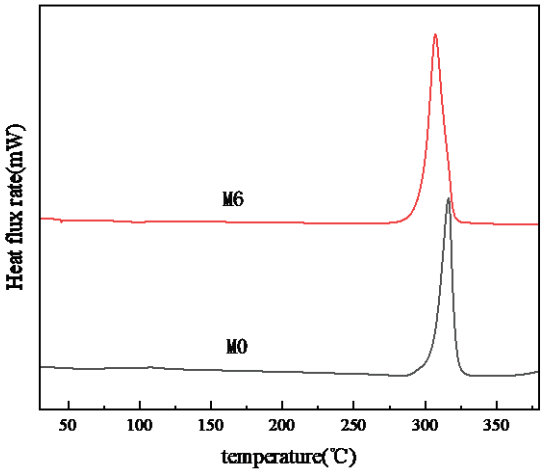

Fig. 5. DSC curves of PAN/PES/TiO_2 ultrafiltration membranes at different hydrolysis temperatures.

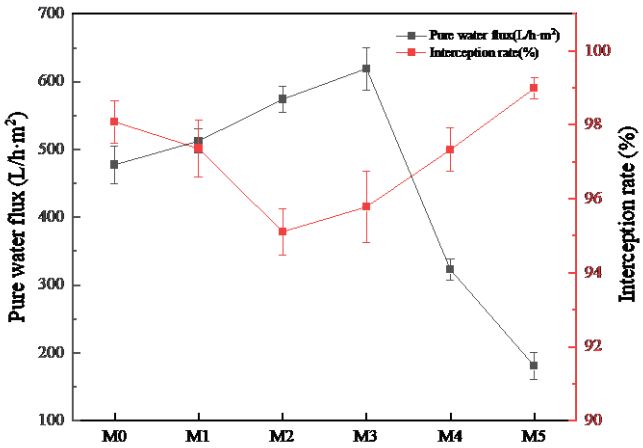

Fig. 6. Trend of water flux and retention rate of PAN/PES/TiO_2 membrane at different hydrolysis temperatures.

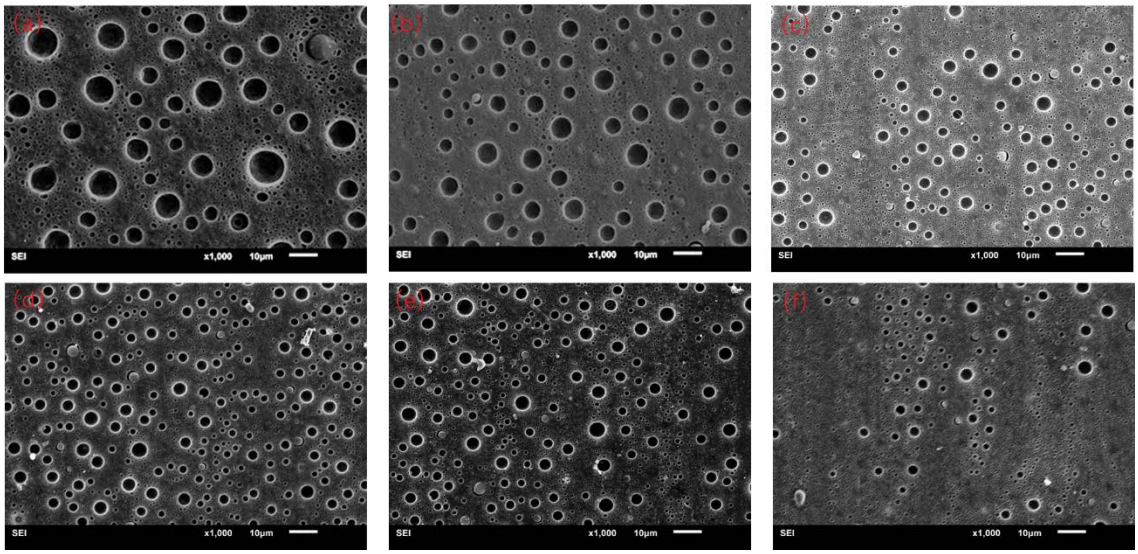

Fig. 7. Surface morphology of PAN/PES/TiO_2 ultrafiltration membranes at different hydrolysis temperatures (a) M0, (b) M1, (c) M2, (d) M3, (c) M4, and (f) M5.

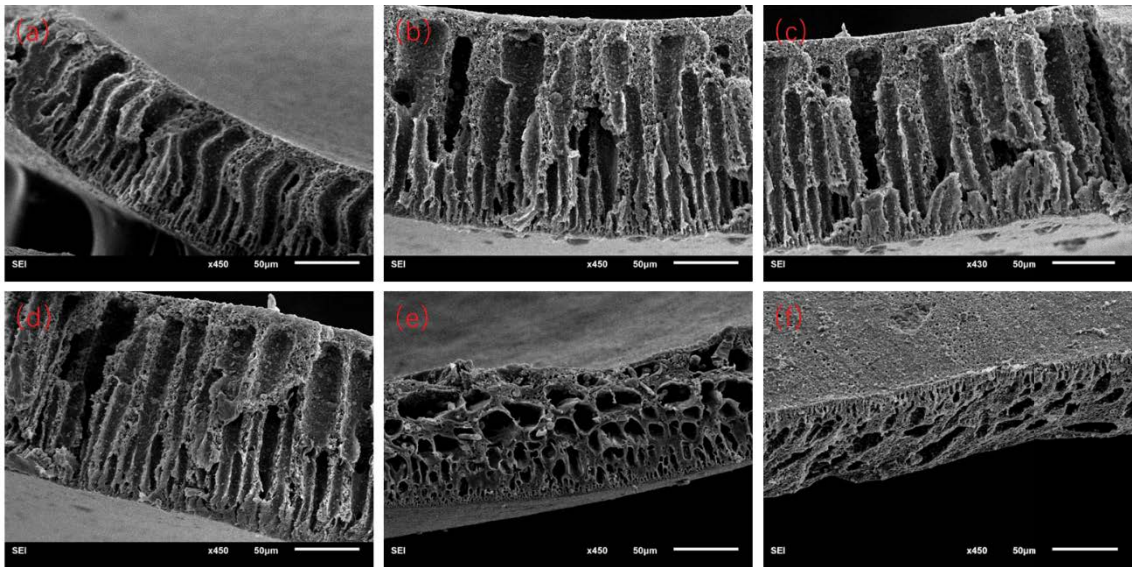

Fig. 8. Cross-sectional view of PAN/PES/TiO_2 ultrafiltration membrane at different hydrolysis temperatures (a) M0, (b) M1, (c) M2, (d) M3, (c) M4, and (f) M5.

have a curved morphology. The membrane has low water permeability, and pollutants are more likely to be blocked inside the membrane. The finger pores of the ultrafiltration membrane are more thorough after hydrolysis modification, which improves the pure water flux of the ultrafiltration membrane. When the hydrolysis temperature is 50°C, the pore structure of the composite membrane is ideal, with an increase in the number of connecting pores at the top and bottom, resulting in finer and denser pores. When the hydrolysis time reaches 50°C, the membrane structure is degraded to some extent due to the excessive hydrolysis and the number of PAN molecular chain breaks. The underlying structure of the membrane is bent and deformed, and the coherent long pores that formed initially virtually all dissolve, creating more circular pore patterns, as shown in the following diagram. When the hydrolysis temperature reaches 60°C, the number of adequate holes suddenly falls, and the large pore structure of the ultrafiltration membrane is filled due to excessive hydrolysis, making water molecules challenging to flow through the interior of the ultrafiltration membrane.

3.5. Effect of alkali hydrolysis temperature on water absorption and porosity of ultrafiltration membrane

Fig. 9 depicts the impact of different hydrolysis temperatures on the water absorption and porosity of PAN/PES/TiO_2 ultrafiltration membranes. The results revealed that

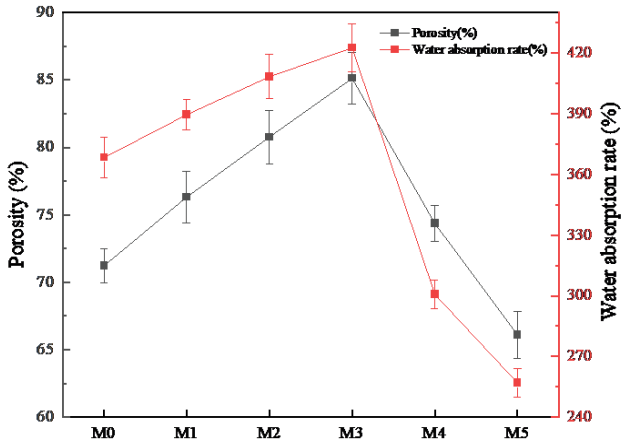

Fig. 9. Trend of porosity and water absorption of PAN/PES/TiO_2 membrane at different hydrolysis temperatures.

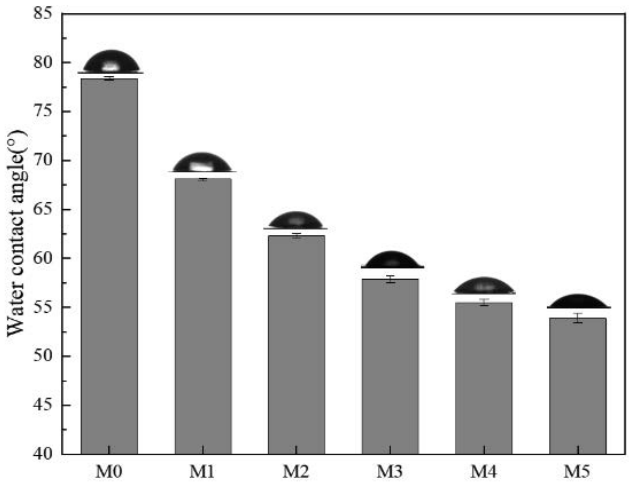

Fig. 10. Trend of contact angle of PAN/PES/TiO_2 film at different hydrolysis temperatures.

when the hydrolysis temperature increased, the porosity and water absorption of the composite membrane increased and eventually declined. The membrane functioned best at a hydrolysis temperature of 50°C, with maximum porosity and water absorption values of 85.12% and 422.16%, respectively. The hydrolysis reaction between PAN and NaOH solution in PAN/PES/TiO_2 composite ultrafiltration membrane forms more hydrophilic carboxylic acid groups, which is the reason for improving membrane performance in the early hydrolysis stage. The alkali hydrolysis reaction becomes more complete as the temperature rises, producing more hydrophilic groups. However, the excessive hydrolysis reaction fills the pore structure of the PAN/PES/TiO_2 ultrafiltration membrane, and the molecular chains of PAN and PES curl due to the high temperature, resulting in ultrafiltration membrane deformation. As a result, when the hydrolysis temperature is above 50°C, the pore size and water absorption of the ultrafiltration membrane decrease. This suggests that various parameters influence the performance of ultrafiltration membranes, and improving the hydrophilicity of ultrafiltration membranes while preserving their internal structure is vital.

3.6. Effect of alkali hydrolysis temperature on the hydrophilicity of ultrafiltration membranes

The impact of alkaline hydrolysis temperature on the surface hydrophilicity of PAN/PES/TiO_2 composite ultrafiltration membranes is investigated in Fig. 10. The results revealed that as the hydrolysis temperature increased, the water contact angle of the composite membrane decreased, indicating that the surface hydrophilicity of the membrane increased. The water contact angle reduces by 26.1% when the hydrolysis temperature exceeds 50°C compared to the composite ultrafiltration membrane without soaking modification. The water contact angle is 31.3% smaller than the composite ultrafiltration membrane without washing modification when the hydrolysis temperature reaches 60°C. The rise in hydrophilicity of ultrafiltration membranes with increasing temperature is attributed to increased hydrophilic groups formed by PAN hydrolysis. Including TiO_2 nanoparticles will improve the hydrolysis effect of ultrafiltration membranes, resulting in improved membrane surface hydrophilicity [42,43]. Infrared spectroscopy analysis and DSC testing support the preceding opinion. However, as the hydrolysis temperature approaches 50°C, the membrane water contact angle reduction reduces because hydrolysis creates more hydrophilic groups, and the hydrophilicity of the membrane is regulated by characteristics such as porosity and pore size. The quantity of surface "small pits" drops off quickly at high hydrolysis temperatures, and the finger-shaped prominent cavity structure is hidden. Scanning electron microscopy and porosity testing can confirm this conclusion. Significant structural alterations in ultrafiltration membranes have made it impossible for water molecules to infiltrate the composite membrane, cancelling out the beneficial benefits of hydrophilic groups. As a result, the hydrophilicity of the membrane surface has not improved considerably in the subsequent step.

3.7. Effect of alkali hydrolysis temperature on static contamination resistance of ultrafiltration membranes

Fig. 11 shows the effect of hydrolysis temperature on the static adsorption capacity of the PAN/PES/TiO_2 composite ultrafiltration membrane. The results revealed that when the hydrolysis temperature increased, the static adsorption capacity of the composite ultrafiltration membrane declined and then increased. Overall, the fixed adsorption amount of the hydrolysis-modified ultrafiltration membrane was lower than that of the unmodified composite membrane. This indicates that hydrolysis modification can significantly improve the surface anti-fouling performance of PAN/PES/TiO_2 composite ultrafiltration membranes. At a hydrolysis temperature of 50°C, the static adsorption quantity was as low as 0.0299 mg/cm^2. When the hydrolysis temperature approached 50°C, static adsorption rose while the anti-pollution impact on the surface reduced. This happens because as the temperature increases, more cyano groups in PAN are hydrolyzed, resulting in more hydrophilic carboxylic acid groups. The increased hydrophilicity promotes the formation

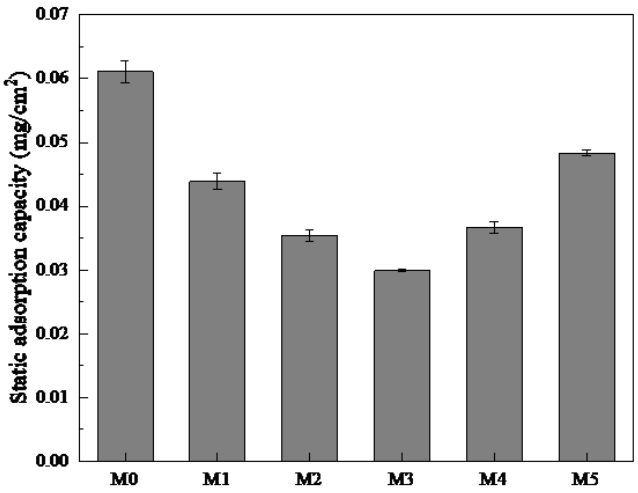

Fig. 11. Trend of static adsorption of PAN/PES/TiO_2 membrane at different hydrolysis temperatures.

of a hydrated layer film on the surface of the ultrafiltration membrane, which improves the anti-pollution performance of the membrane, and the addition of self-cleaning material TiO_2 nanoparticles improves the anti-pollution performance of the composite ultrafiltration membrane even further. However, when the hydrolysis temperature rose over 50°C, the membrane surface roughened, and the surface area of the membrane in contact with pollutants increased, resulting in a loss of the static anti-pollution effect of the ultrafiltration membrane.

3.8. Effect of alkali hydrolysis temperature on the contamination resistance factor of ultrafiltration membrane

Ultrafiltration membrane contamination resistance is an essential indicator of membrane applicability, and membrane anti-pollution performance directly impacts service life and application breadth. The trend of each anti-pollution coefficient of the composite membrane is shown in Table 2. The results showed that as the hydrolysis temperature increased, the *m* and Rir values of the ultrafiltration membrane decreased while the Rr value increased. It implies that the modification method of increasing hydrolysis temperature can improve the anti-pollution property of the ultrafiltration membrane. This contrasts the preceding trend of static anti-pollution performance, which is boosted initially and subsequently diminished because dynamic anti-pollution has a backwashing process, and inevitable impurities adhering to the membrane surface are eliminated by simple cleaning with deionized water. The PAN/PES/TiO_2 composite ultrafiltration membrane has the most miniature m and Rir when the hydrolysis temperature reaches 60°C, 0.03704, and 3.571%, respectively. The Rr value of the membrane reached a maximum of 37.5% at the hydrolysis temperature of 50°C, and it changed very little after this temperature was exceeded. The primary cause of these events is that when the temperature rises, the hydrolysis process between PAN and NaOH becomes more complete, forming more hydrophilic groups. Simultaneously, the addition of

Table 2
Anti-contamination performance parameters of PAN/PES/TiO_2 membranes at different hydrolysis temperatures

	m	Rr (%)	Rir (%)
M0	0.3455	32.43	25.68
M1	0.2951	34.18	22.78
M2	0.2192	35.96	17.98
M3	0.1429	37.5	12.5
M4	0.1364	25	12
M5	0.03704	24	3.57

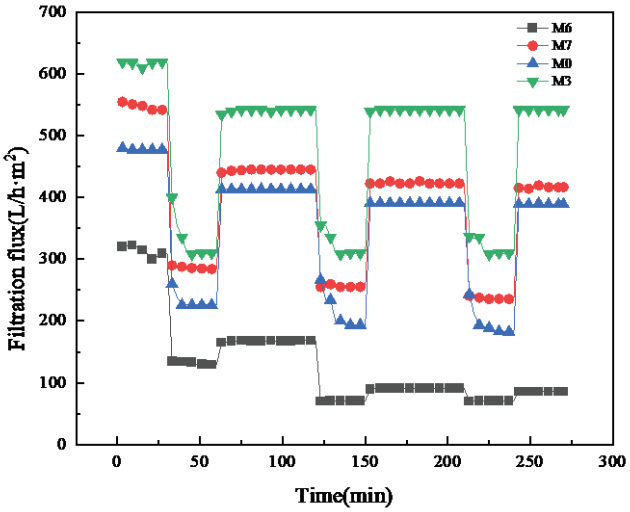

Fig. 12. Three-cycle filtration fluxes of different substrate membranes after hydrolysis modification.

hydrophilic inorganic filler TiO_2 nanoparticles improves the hydrophilicity of the hydrolyzed ultrafiltration membrane, improving the transport ability of water molecules through the pores of the composite ultrafiltration membrane, increasing the water flux of the membrane and making it difficult for pollutants to adhere to the membrane surface, causing membrane fouling. Specifically, complete the ultrafiltration membrane self-cleaning [44,45].

3.9. Comparison of the anti-pollution stability of different components of ultrafiltration membranes

Fig. 12 shows the dynamic schematic diagram of ultrafiltration membranes with different components undergoing three flux cycles, where PAN/PES hydrolysis membranes were modified by immersion at 50°C for 60 min, and PAN/PES/TiO_2 hydrolysis membranes were changed by immersion at 50°C for 45 min. BSA was employed as a contamination model in the tests to examine the stability of ultrafiltration membranes against contamination. The results showed that the PAN/PES ultrafiltration membrane caused a decrease in filtration flux after each cycle of the test. Still, the decline in filtration flux of the PAN/PES hydrolysis membrane and PAN/PES/TiO_2 ultrafiltration membrane

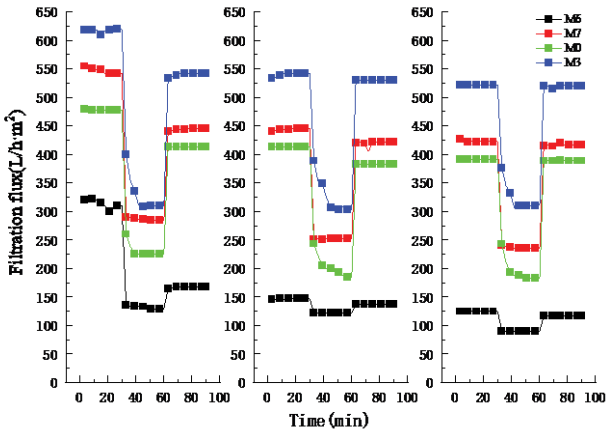

Fig. 13. Filtration flux of ultrafiltration membranes at different placement times (a) Initial membrane filtration flux, (b) ultrafiltration membrane filtration flux after three months of placement, and (c) ultrafiltration membrane filtration flux after six months of placement.

was significantly reduced, especially the filtration flux of the PAN/PES/TiO_2 hydrolysis membrane. Both surface hydrolysis and blending procedures can increase the hydrophilicity of ultrafiltration membranes, which is why both occurrences occur. According to research, including TiO_2 inorganic fillers can increase the stability of ultrafiltration membranes and significantly improve their hydrophilicity. The increase in hydrophilicity might make the membrane surface more readily saturated with water molecules, forming a "hydrated layer" film. This thin layer not only acts as a pollution barrier but also improves the anti-pollution stability of the ultrafiltration membrane, which is critical for extending the service life of the membrane and lowering maintenance costs [46].

3.10. Filtration flux stability test of ultrafiltration membranes with different components

Fig. 13 compares the filtration fluxes of various fractions of ultrafiltration membranes after 3 d (a), three months (b), and six months (c) of deployment. The results showed that the anti-pollution stability of ultrafiltration membranes with different modifications was improved compared to PAN/PES ultrafiltration membranes. In particular, the filtration flux of the PAN/PES/TiO_2 hydrolysis membranes was hardly reduced, which indicates that the anti-pollution stability of the ultrafiltration membranes was finally modified by a combination of modifications (surface modification and co-blending modification) was improved. The main reason for this phenomenon is that the hydrolysis modification and the co-blending incorporation of TiO_2 nanoparticles can introduce hydrophilic groups, such as carboxyl groups and hydroxyl groups, which will strongly interact with water to form an anti-fouling shield and reduce the probability of contaminants falling on the ultrafiltration membrane surface. Even if some pollutants adhere to the membrane surface, the force between them and the membrane is feeble and can be removed by a simple rinse [23]. The ultrafiltration membrane can be endowed with self-cleaning ability using such compound modification. Hence, the filtration performance of the PAN/PES/TiO_2 hydrolysis membrane still performs well after six months of placement [47].

Table 3
Glass transition temperature (T_g) of different component ultrafiltration membranes

	T_g (°C)
M0	104.16
M6	99.39
M8	95.09
M9	225.35

3.11. Thermal properties of membranes

Blended polymers with good compatibility will display a T_g value between the polymers [48]. As shown in Table 3, the T_g values of M0 and M6 are between M8 and M9 ultrafiltration membranes, and all ultrafiltration membranes have only a single T_g value. Moreover, adding TiO_2 nanoparticles will to some extent, enhance the T_g of PAN/PES ultrafiltration membranes. This is because TiO_2 nanoparticles have a higher T_g, and when blended with other materials with good compatibility, the T_g of the blend will increase. TiO_2 nanoparticles will agglomerate when compatibility is poor, leading to a decrease in T_g. In summary, PAN, PES, and TiO_2 nanoparticles have good compatibility.

4. Conclusion

This study used a phase inversion method to prepare a PAN/PES/TiO_2 composite ultrafiltration membrane and hydrophilic modification of the membrane was carried out using a low-concentration NaOH solution. After thoroughly examining the modification conditions of alkali hydrolysis, the optimum hydrolysis temperature of 50°C was established. The pure water flux of M3 achieved 619.4 L/m²·h, an improvement of 29.7% over the unmodified M0. In addition, the surface hydrophilicity and pollution resistance of the hydrolysis-modified membrane and porosity were significantly improved. Meanwhile, under the same working conditions, we created PAN/PES ultrafiltration membranes and PAN/PES-50°C, and the four separate components of ultrafiltration membranes were tested for performance stability. The results showed that M3 performed admirably in the anti-pollution and long-term flux stability tests. This suggests that combining alkali hydrolysis surface modification and co-blending with hydrophilic TiO_2 nanoparticles can significantly improve the overall performance of ultrafiltration membranes, particularly anti-pollution and long-term flux stability. This will present a fresh research proposal for extending the service life and lowering the cost of ultrafiltration membrane maintenance.

Symbols

J_w	—	Water flux, L/m²·h
V	—	Volume of water passing through the membrane, L
S_1	—	Effective filtration area, m²

Δt	—	Collection time, h
R	—	Interception rate, %
C_1	—	Absorbance of BSA in filtrate
C_0	—	Absorbance of BSA in feeding liquid
Pr	—	Porosity, %
W_1	—	Composite film wet weight, g
W_2	—	Composite film dry weight, g
V_m	—	Composite membrane volume, cm^3
ϱ	—	Water density, g/cm^3
W	—	Water absorption rate, %
W_w	—	Ultrafiltration membrane wet weight, g
W_d	—	Ultrafiltration membrane dry weight, g
C	—	Solution concentration, mg/L
A	—	Absorbance of the solution at 278.5 nm
Q	—	Static adsorption capacity, mg/cm^2
V_1	—	Volume of BSA solution, L
S_2	—	Ultrafiltration membrane area, cm^2
m	—	Total fouling coefficient of membrane
Rr	—	Reversible fouling coefficient of membrane, %
Rir	—	Irreversible fouling coefficient of membrane, %

References

[1] W. Tang, Y. Pei, H. Zheng, Y. Zhao, L. Shu, H. Zhang, Twenty years of China's water pollution control: experiences and challenges, Chemosphere, 295 (2022) 133875, doi: 10.1016/j.chemosphere.2022.133875.

[2] M. Mergili, J.P. Müller, J.F. Schneider, Spatio-temporal development of high-mountain lakes in the headwaters of the Amu Darya River (Central Asia), Global Planet. Change, 107 (2013) 15–17.

[3] S. Hube, M. Eskafi, K.F. Hrafnkelsdóttir, B. Bjarnadóttir, M.Á. Bjarnadóttir, S. Axelsdóttir, B. Wu, Direct membrane filtration for wastewater treatment and resource recovery: a review, Sci. Total Environ., 710 (2020) 7–10.

[4] Z. Chen, Q. Wu, G. Wu, H.Y. Hu, Centralized water reuse system with multiple applications in urban areas: lessons from China's experience, Resour. Conserv. Recycl., 117 (2017) 125–136.

[5] S. Bauer, H.J. Linke, M. Wagner, S. Bauer, H.J. Linke, M. Wagner, Combining industrial and urban water-reuse concepts for increasing the water resources in water-scarce regions, Water Environ. Res., 92 (2020) 1027–1028.

[6] S.B. Teli, S. Molina, E.G. Calvo, A.E. Lozano, J. de Abajo, Preparation, characterization and antifouling property of polyethersulfone-PANI/PMA ultrafiltration membranes, Desalination, 299 (2012) 113–114.

[7] S.G. Ding, X.Q. Cheng, Z.X. Jiang, Y.P. Bai, L. Shao, Pore morphology control and hydrophilicity of polyacrylonitrile ultrafiltration membranes, J. Appl. Polym. Sci., 132 (2015) 11–12.

[8] B. Said, S. M'rabet, R. Hsissou, A. El Harfi, Synthesis of new low-cost organic ultrafiltration membrane made from polysulfone/polyetherimide blends and its application for soluble azoic dyes removal, J. Mater. Res. Technol., 9 (2020) 4763–4772.

[9] B. Saini, M.K. Sinha, Effect of hydrophilic poly(ethylene glycol) methyl ether additive on the structure, morphology, and performance of polysulfone flat sheet ultrafiltration membrane, J. Appl. Polym. Sci., 136 (2019) 12–14.

[10] M.R. Raviya, M.V. Gauswami, H.D. Raval, A novel polysulfone/iron-nickel oxide nanocomposite membrane for removal of heavy metal and protein from water, Water Environ. Res., 92 (2020) 1990–1991.

[11] S.G. Ouyang, J.Y. Yao, G.H.W. Zhu, Z.Y. Liu, C. Feng, G. Wang, Hydrophilic modification of a poly(ether sulfone) flat-sheet ultrafiltration membrane applied to coking sewage, J. Appl. Polym. Sci., 134 (2017) 3–6.

[12] S. Zhao, Z. Wang, J. Wang, S. Wang, Poly(ether sulfone)/polyaniline nanocomposite membranes: effect of nanofiber size on membrane morphology and properties, Ind. Eng. Chem. Res., 53 (2014) 11468–11477.

[13] S.S. Hosseini, T.S. Fakharian, M. Alaei Shahmirzadi, T. Tavangar, Fabrication, characterization, and performance evaluation of polyethersulfone/TiO_2 nanocomposite ultrafiltration membranes for produced water treatment, Polym. Adv. Technol., 29 (2018) 2619–2620.

[14] W. Zhao, L. Liu, L. Wang, N. Li, Functionalization of polyacrylonitrile with tetrazole groups for ultrafiltration membranes, RSC Adv., 6 (2016) 72133–72134.

[15] J. Jegal, K.H. Lee, Chitosan membranes crosslinked with sulfosuccinic acid for the pervaporation separation of water/alcohol mixtures, J. Appl. Polym. Sci., 71 (1999) 671–675.

[16] B. Jung, J.K. Yoon, B. Kim, H.W. Rhee, Effect of molecular weight of polymeric additives on formation, permeation properties and hypochlorite treatment of asymmetric polyacrylonitrile membranes, J. Membr. Sci., 243 (2004) 45–46.

[17] X. Yang, S.R. Liew, R. Bai, Simultaneous alkaline hydrolysis and non-solvent induced phase separation method for polyacrylonitrile (PAN) membrane with highly hydrophilic and enhanced anti-fouling performance, J. Membr. Sci., 635 (2021) 119499, doi: 10.1016/j.memsci.2021.119499.

[18] K.I. Moideen, A.M. Isloor, A.F. Ismail, A. Obaid, H.K. Fun, Fabrication and characterization of new PSF/PPSU UF blend membrane for heavy metal rejection, Desal. Water Treat., 57 (2016) 19810–19819.

[19] J. Zhang, Y.N. Xu, S. Chen, J. Li, W. Han, X. Sun, L. Wang, Enhanced antifouling and antibacterial properties of poly(ether sulfone) membrane modified through blending with sulfonated poly(aryl ether sulfone) and copper nanoparticles, Appl. Surf. Sci., 434 (2018) 806–815.

[20] Y. Qin, H. Yang, Z. Xu, F. Li, Surface modification of polyacrylonitrile membrane by chemical reaction and physical coating: comparison between static and pore-flowing procedures, ACS Omega, 3 (2018) 4231–4241.

[21] X. Zhang, C Xiao, X. Hu, Preparation and properties of polysulfone/polyacrylonitrile blend membrane and its modification with hydrolysis, Desal. Water Treat., 511 (2013) 3979–3987.

[22] C.C. Chang, K.G. Beltsios, J.D. Lin, L.P. Cheng, Nano-titania/polyethersulfone composite ultrafiltration membranes with optimized antifouling capacity, J. Taiwan Inst. Chem. Eng., 113 (2020) 325–327.

[23] S.N.W. Ikhsan, N. Yusof, F. Aziz, N. Misdan, A.F. Ismail, W.J. Lau, N.H.H. Hairom, Efficient separation of oily wastewater using polyethersulfone mixed matrix membrane incorporated with halloysite nanotube-hydrous ferric oxide nanoparticle, Sep. Purif. Technol., 199 (2018) 161–165.

[24] S.S. Madaeni, N. Ghaemi, Characterization of self-cleaning RO membranes coated with TiO_2 particles under UV irradiation, J. Membr. Sci., 303 (2007) 221–233.

[25] K. Feng, L. Hou, B. Tang, P. Wu, A self-protected self-cleaning ultrafiltration membrane by using polydopamine as a free-radical scavenger, J. Membr. Sci., 490 (2015) 120–128.

[26] H. Song, J. Shao, Y. He, B. Liu, X. Zhong, Natural organic matter removal and flux decline with PEG-TiO_2-doped PVDF membranes by integration of ultrafiltration with photocatalysis, J. Membr. Sci., 405 (2012) 48–56.

[27] J. Wang, Z. Yue, J.S. Ince, J. Economy, Preparation of nanofiltration membranes from polyacrylonitrile ultrafiltration membranes, J. Membr. Sci., 286 (2006) 333–336.

[28] G. Zhang, H. Meng, S. Ji, Hydrolysis differences of polyacrylonitrile support membrane and its influences on polyacrylonitrile-based membrane performance, Desalination, 242 (2009) 313–324.

[29] C.L. Lai, W.C. Chao, W.S. Hung, Q. An, M. De Guzman, C.C. Hu, K.R. Lee, Physicochemical effects of hydrolyzed asymmetric polyacrylonitrile membrane microstructure on dehydrating butanol, J. Membr. Sci., 490 (2015) 275–281.

[30] Y.H. Choi, C.M. Choi, D.H. Choi, Y. Paik, B.J. Park, Y.K. Joo, N.J. Kim, Time dependent solid-state ^{13}C NMR study on alkaline hydrolysis of polyacrylonitrile hollow fiber ultrafiltration membranes, J. Membr. Sci., 371 (2011) 84–89.

[31] R. Cheraghali, Z. Maghsoud, Enhanced modification technique for polyacrylonitrile UF membranes by direct hydrolysis in

the immersion bath, J. Appl. Polym. Sci., 137 (2020) 48583, doi: 10.1002/app.48583.
[32] J. Coca, Proceedings of the NATO Advanced Training Course on Water Purification and Management in Mediterranean Countries, Springer, Netherlands, Oviedo, 2008.
[33] J. Kong, K. Li, Oil removal from oil-in-water emulsions using PVDF membranes, Sep. Purif. Technol., 16 (1999) 83–93.
[34] B.T. Konvensional, A review of oilfield wastewater treatment using membrane filtration over conventional technology, Malays. J. Anal., 21 (2017) 643–658.
[35] D.J. Miller, S. Kasemset, D.R. Paul, B.D. Freeman, Comparison of membrane fouling at constant flux and constant transmembrane pressure conditions, J. Membr. Sci., 454 (2014) 505–515.
[36] T. Zhang, F.X. Kong, X.C. Li, Q. Liu, J.F. Chen, C.M. Guo, Comparison of the performance of prepared pristine and TiO_2 coated UF/NF membranes for two types of oil-in-water emulsion separation, Chemosphere, 244 (2020) 125386, doi: 10.1016/j.chemosphere.2019.125386.
[37] A. Rahimpour, S.S. Madaeni, A.H. Taheri, Y. Mansourpanah, Coupling TiO_2 nanoparticles with UV irradiation for modification of polyethersulfone ultrafiltration membranes, J. Membr. Sci., 313 (2008) 158–169.
[38] S.Y. Jin, M.H. Kim, Y.G. Jeong, Y.I. Yoon, W.H. Park, Effect of alkaline hydrolysis on cyclization reaction of PAN nanofibers, Mater. Des., 124 (2017) 69–77.
[39] C. Han, Q. Liu, Q. Xia, Y. Wang, Facilely cyclization-modified PAN nanofiber substrate of thin film composite membrane for ultrafast polar solvent separation, J. Membr. Sci., 641 (2022) 119911, doi: 10.1016/j.memsci.2021.119911.
[40] T.H. Elagib, E.A. Hassan, B. Liu, K. Han, M. Yu, Evaluation of composite PAN fibers incorporated with carbon nanotubes and titania and their performance during the microwave-induced pre-oxidation, Carbon Lett., 30 (2020) 235–245.
[41] R. Zhou, D. Rana, T. Matsuura, C.Q. Lan, Effects of multi-walled carbon nanotubes (MWCNTs) and integrated MWCNTs/SiO_2 nano-additives on PVDF polymeric membranes for vacuum membrane distillation, Sep. Purif. Technol., 217 (2019) 154–163.
[42] V. Murugesan, D. Rana, T. Matsuura, C.Q. Lan, Optimization of nanocomposite membrane for vacuum membrane distillation (VMD) using static and continuous flow cells: effect of nanoparticles and film thickness, Sep. Purif. Technol., 241 (2020) 9–10.
[43] Z. Li, D. Rana, T. Matsuura, C.Q. Lan, The performance of polyvinylidene fluoride-polytetrafluoroethylene nanocomposite distillation membranes: an experimental and numerical study, Sep. Purif. Technol., 226 (2019) 192–208.
[44] S.S. Hosseini, S.T. Fakharian, M.A.A. Shahmirzadi, T. Tavangar, Fabrication, characterization, and performance evaluation of polyethersulfone/TiO_2 nanocomposite ultrafiltration membranes for produced water treatment, Polym. Adv. Technol., 29 (2018) 2619–2631.
[45] Y. Li, X. Yang, Y. Wen, Y. Zhao, L. Yan, G. Han, L. Shao, Progress reports of mineralized membranes: engineering strategies and multifunctional applications, Sep. Purif. Technol., 304 (2023) 122379, doi: 10.1016/j.seppur.2022.122379.
[46] L. Yan, X. Yang, H. Zeng, Y. Zhao, Y. Li, X. He, L. Shao, Nanocomposite hydrogel engineered hierarchical membranes for efficient oil/water separation and heavy metal removal, J. Membr. Sci., 668 (2023) 8–10.
[47] Y. Wen, X. Yang, Y. Li, L. Yan, Y. Zhao, L. Shao, Progress reports of metal-phenolic network engineered membranes for water treatment, Sep. Purif. Technol., 320 (2023) 124225, doi: 10.1016/j.seppur.2023.124225.
[48] V.A. Pham, J.P. Santerre, T. Matsuura, R.M. Narbaitz, Application of surface modifying macromolecules in polyethersulfone membranes: influence on PES surface chemistry and physical properties, J. Appl. Polym. Sci., 73 (1999) 1363–1378.